

¹³A. E. Lord and D. N. Beshers, *Acta Met.* **14**, 1659 (1966).

¹⁴C. G. Homan and J. F. Cox, in *Physics of Solids at High Pressures*, edited by C. T. Tomizuka and R. M. Emrick (Academic, New York, 1965).

¹⁵H. Jujiwara, T. Okamoto, and E. Tatsumoto, in *Physics of Solids at High Pressures*, edited by C. T. Tomizuka and R. M. Emrick (Academic, New York 1965).

¹⁶E. S. Fisher and D. Dever, *Trans. AIME* **239**, 48 (1967).

¹⁷S. Diamond and C. A. Wert, *Trans. AIME* **239**, 705 (1967).

¹⁸W. Hampe and D. Widman, *Z. Angew. Phys.* **15**, 360 (1963).

¹⁹B. Pegel, *Phys. Status Solidi* **22**, 223 (1967).

²⁰B. Pegel, *Phys. Status Solidi* **22**, K45 (1967).

²¹C. Wert and C. Zener, *Phys. Rev.* **76**, 1169 (1949).

²²J. Stanley and C. Wert, *J. Appl. Phys.* **32**, 267 (1961).

²³D. Lazarus, *Solid State Phys.* **10**, 71 (1960).

²⁴C. P. Flynn and A. M. Stoneham, *Phys. Rev. B* **1**, 3966 (1970).

²⁵D. E. Temkin, *Fiz. Metal. Metalloved. (USSR)* **29**, 589 (1970).

²⁶Concerning the value of $11.3 \text{ cm}^3 \text{ mole}^{-1}$ (Ref. 14), it is noted that the value of δ_T of ferromagnetic solids close to the Curie temperature is often quite large and negative [H. Ebert and A. Kussman, *Z. Physik* **38**, 437 (1937)]. If this is the case for iron, a value of $11.3 \text{ cm}^3 \text{ mole}^{-1}$ might not disagree with the magnetic energy model.

PHYSICAL REVIEW B

VOLUME 3, NUMBER 3

1 FEBRUARY 1971

Magnetic Structure of RbMnCl_3

M. Melamud, J. Makovsky, and H. Shaked

Nuclear Research Centre - Negev, P.O.B. 9001, Beer-Sheva, Israel

and

S. Shtrikman

Weizmann Institute of Science, Department of Electronics, Rehovot, Israel

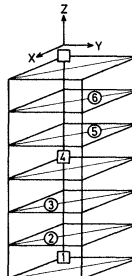
(Received 24 July 1970)

The compound RbMnCl_3 is paramagnetic at room temperature and belongs to the space group $D_{6h}^4-P6_3/mmc$ with six molecules per unit cell. Neutron diffraction of RbMnCl_3 -powder sample was studied as a function of the sample temperature. A transition to antiferromagnetism was found at $T_N \sim 94^\circ\text{K}$. The magnetic structure determined from the diffraction pattern at 4.2°K consists of ferromagnetic planes stacked in the sequence $A(+)$, $B(-)$, $B(+)$, $A(-)$, $C(+)$, $C(-)$, along the c axis. Spin direction is perpendicular to the c axis, defining an infinite number of structures which belong to a two-dimensional irreducible representation Γ_6^* of D_{6h}^4 . Two distinctly different structures of orthorhombic symmetry, $Cm'c'm$ and $Cmcm$, span the subspace of this representation and are consistent with the diffraction data. Dipolar energy calculations show that the direction perpendicular to the \hat{z} direction is of lower dipolar energy than that parallel to \hat{z} . The existence of a spin component perpendicular to \hat{z} is also confirmed with the aid of an external magnetic field. A magnetic moment of $4.1 \mu_B$ is calculated for the Mn^{2+} ion from the diffraction pattern at 4.2°K .

INTRODUCTION

The compound RbMnCl_3 was previously investigated by means of x rays,¹⁻³ and by paramagnetic and antiferromagnetic resonance.^{4,5} It was reported^{1,2} to be of the hexagonal BaTiO_3 type, which belongs to the space group $D_{6h}^4-P6_3/mmc$, with six formula units per unit cell. ($a_0 = 7.164$, $c_0 = 17.798$, $c_0/a_0 = 2.484$ ¹; $a_0 = 7.165$, $c_0 = 17.815$, $c_0/a_0 = 2.486$ ². These values are in agreement within their error limits.) The six magnetic ions in this structure occupy the $2a$ and $4f$ sites (Fig. 1). According to Tiskhchenko,³ RbMnCl_3 belongs to the same space group, but has only two formula units per unit cell, and therefore is of the CsNiCl_3 type. We shall see below that our data are consistent with the BaTiO_3 -type structure and are inconsistent with the

CsNiCl_3 -type structure. RbMnCl_3 was reported to be antiferromagnetic¹ with the spins of the Mn^{2+} ions



	COORDINATES	SITE	PLANE
①	1/3 2/3 5/6	4f	C(-)
②	1/3 2/3 2/3	4f	C(+)
③	0 0 1/2	2a	A(-)
④	2/3 1/3 1/3	4f	B(+)
⑤	2/3 1/3 1/6	4f	B(-)
⑥	0 0 0	2a	A(+)

FIG. 1. Positions of Mn^{2+} ions in the unit cell. A, B, C denote the threefold axes on which the ions are placed.

lying in the plane perpendicular to the c axis,⁵ with a Néel temperature of $(86 \pm 6)^\circ \text{K}$.⁴ We report here the results of neutron-diffraction measurements of RbMnCl_3 powder in the range from liquid-helium to room temperature, and the magnetic structure deduced from these results.

The two isostructural fluorides CsMnF_3 and RbNiF_3 were also reported⁶⁻⁸ to order antiferromagnetically, with the spin axis perpendicular to the c axis. The compound RbNiF_3 , unlike CsMnF_3 and RbMnF_3 , was found⁸ to exhibit a spontaneous magnetic moment.

EXPERIMENTAL

Stoichiometric amounts of RbCl and anhydrous MnCl_2 were weighed into a quartz ampoule. The ampoule, after being evacuated and sealed, was heated up to about 600°C and left at this temperature for a few hours. Chemical analysis of the manganese and chlorine content of the resulting orange-colored compound was carried out by the ethylene-diamine tetra-acetic acid (EDTA) complexometric titration and argentometric titration, respectively. Results of the analysis are Mn^{2+} , 22.35% (calc. 22.26%); Cl^- , 42.96% (calc. 43.10%). An x-ray powder diagram of the material yielded lines of the pure compound only.¹

The temperature dependence of the magnetic susceptibility of a powder sample of this preparation was measured on a vibrating sample magnetometer (VSM) and showed an antiferromagnetic transition at $(95 \pm 2)^\circ \text{K}$. A paramagnetic moment $\mu_{\text{eff}} \sim 5.3 \mu_B$ was calculated from the slope of χ_m^{-1} above 250°K .

Neutron ($\lambda = 1.03 \text{ \AA}$) powder-diffraction patterns were obtained at room, liquid-nitrogen, and liquid-

helium temperatures; the last two show reflections from a magnetically ordered structure in addition to the nuclear reflections of the room-temperature pattern. The neutron-diffraction patterns at room and liquid-helium temperatures are shown in Fig. 2. The patterns were indexed according to the unit cell with six formula units per cell with $a_0 = 7.164$, $c_0 = 17.79 \text{ \AA}$.¹ These patterns could not be indexed according to the unit cell with two formula units per cell.³

There are two low-scattering-angle lines $\{100\} + \{003\} + \{101\}$ and $\{102\}$, which are purely magnetic. The intensity of the $\{100\} + \{003\} + \{101\}$ line was measured as a function of temperature (Fig. 3). A Néel temperature of $(94 \pm 2)^\circ \text{K}$ was obtained from this measurement. A similar measurement of the intensity of the $\{102\}$ line yielded the same Néel temperature.

The high-scattering-angle nuclear reflections in the diffraction pattern, with the sample at liquid-helium temperature, exhibit some line broadening (Fig. 2). We suspect that this is caused by a distortion of the crystallographic structure. Aside from the broadening, there is a slight shift of the lines to higher scattering angles resulting from thermal contraction of the unit cell.

The intensities of the magnetic lines $\{100\} + \{003\} + \{101\}$ and $\{102\}$ have been measured in a constant magnetic field of about 6 kOe parallel to the scattering vector, with the sample at liquid-nitrogen temperature. An increase of $\sim 15\%$ with respect to the zero-field intensities was detected. An increase is expected as a result of a redistribution of the population of domains only if the spin direction is perpendicular to the hexagonal axis. The

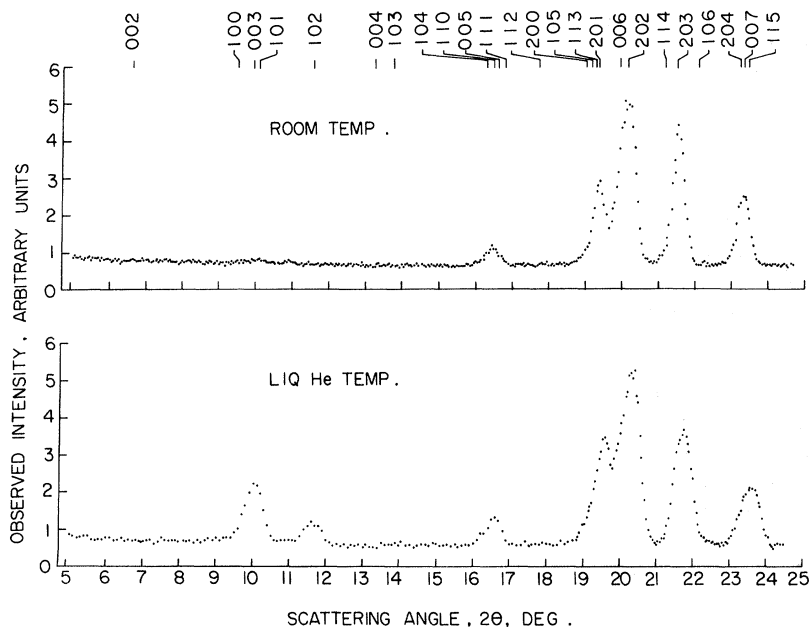


FIG. 2. Observed neutron ($\lambda = 1.03 \text{ \AA}$) diffraction patterns of RbMnCl_3 powder. Indexing is according to the hexagonal unit cell with $a_0 = 7.164$ and $c_0 = 17.79 \text{ \AA}$.

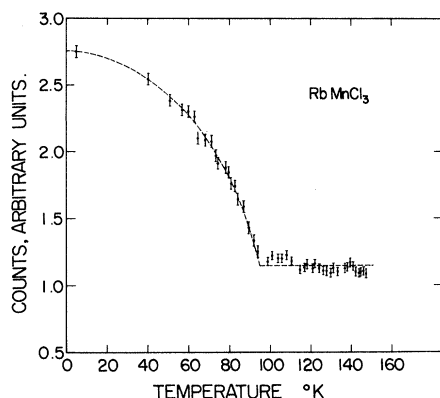


FIG. 3. Temperature dependence of the integrated intensity of the $\{100\} + \{003\} + \{101\}$ magnetic line of RbMnCl_3 .

calculated increase at saturation is 36 and 50% for the first and second lines, respectively.

ANALYSIS OF RESULTS AND DISCUSSION

Our first step is to establish the crystallographic and magnetic unit cells. The indexing of the neutron-diffraction patterns (Fig. 2) is in agreement with the unit-cell dimensions given by Kestigian *et al.*¹ and Seifert and Koknat.² The line at $2\theta = 23^\circ 30'$ cannot be indexed on the basis of Tishchenko's data.⁹ From the fact that the magnetic lines can be indexed according to the crystallographic unit cell, we conclude that the magnetic and crystallographic unit cells are identical. The anti-

REPS. AND SHUBNIKOV GROUPS	2a SITE	4f SITE
Γ_2^+ $P6_3/m'm'c'$		
Γ_3^+ $P6_3/m'm'c'$		
Γ_5^+ C $m'c'm'$		
Γ_5^+ C $m'c'm'$		
Γ_6^+ C $m'c'm'$		
Γ_6^+ C $m'c'm'$		
Γ_2^- $P6_3/m'm'c'$		
Γ_3^- $P6_3/m'm'c'$		
Γ_5^- C $m'c'm'$		
Γ_5^- C $m'c'm'$		
Γ_6^- C $m'c'm'$		
Γ_6^- C $m'c'm'$		

FIG. 4. Basis vectors and their Shubnikov groups for the irreducible representations of $D_{6h}^4 - P6_3/m'm'c'$ in the spin spaces of the $2a$ and $4f$ sites.

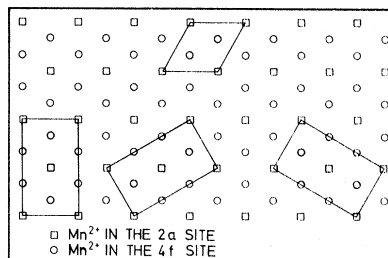


FIG. 5. Projection of the Mn^{2+} sites on the basal plane, in RbMnCl_3 . The hexagonal P cell and the three possible choices of an orthorhombic C cell are shown.

ferromagnetic structures consistent with the latter conclusion are only those obtained by stacking ferromagnetic planes along the c axis. Our second step is to enumerate the possible magnetic structures having magnetic unit cells equal to the crystallographic unit cell. To do this we first consider all the irreducible representations of the space group $D_{6h}^4 - P6_3/m'm'c'$ in the spin spaces of the $2a$ and $4f$ sites. These representations with the corresponding Shubnikov groups are shown in Fig. 4. A general discussion of the methods used to obtain the irreducible representations and their application to magnetic-structure determination was given by Bertaut.¹⁰ It is evident from Fig. 4 that the one-dimensional representations lead to structures of hexagonal symmetry, whereas the two-dimensional representations lead to structures of orthorhombic symmetry in which the paramagnetic sixfold axis is lost. The (001) projections of the corresponding (paramagnetic) hexagonal and (magnetic) orthorhombic unit cells are shown in Fig. 5. Every choice represents a structure and its time conjugate, altogether six structures which transform into one another under the operations of the paramagnetic sixfold axis and under time inversion. These six structures represent six domains in agreement with the phase rule which states that the number of domain is equal to the order of the factor group of the paramagnetic group with respect to the magnetic group. The two partners (six domains for each) of a given representation (i. e., $Cm'cm'$ and $Cmc'm'$ in Γ_5^+) are distinctly different. That is, with single-domain single-crystal data it is possible to tell the difference between the two partners. Unfortunately, in multidomain-diffraction data only the angle the spin makes with the unique axis can be determined,¹¹ hence there is no way of telling from our data to which partner the structure belongs. In the framework of the theory of second-order phase transitions (SOPT) the magnetic structure must belong to a single irreducible representation (see next paragraph). All such structures derived from the irreducible representations of Fig. 4 are listed in the upper half

of Table I. In the lower half of this table, structures in which the two sites transform according to different representations are listed. These structures (lower half) are not allowed by the theory of SOPT. In fact, Table I contains all the collinear structures having the magnetic cell equal to the crystallographic cell which can be constructed from the irreducible representations of $P6_3/mmc$. We have thus enumerated 36 magnetic structures. In the third step, we rule out as many structures as possible on the basis of line extinctions and magnetic measurements. As demonstrated in Table I, 31 structures can be ruled out on the basis of line extinctions alone. Of the five structures left, two are ferromagnetic and therefore inconsistent with VSM and neutron-diffraction measurements. The three possible structures left are $(-\Gamma_6^+, \Gamma_6^+)$, $(-\Gamma_3^+, \Gamma_3^+)$ and $(0, \Gamma_3^-)$ (for notation see Table I).

TABLE I. The 36 possible collinear magnetic structures derived from the basis vectors listed in Fig. 4. Upper or lower halves of the table contain structures in which the spins in the $2a$ and $4f$ sites transform according to the same or different representation, respectively. Reflections listed at the top of the table are absent in our experimental data. Structures for which any of these absences are violated in our calculations of the intensities are checked in the proper column. FO, FI, and AF stand for ferromagnetic, ferrimagnetic, and antiferromagnetic, respectively. The plus or minus signs in front of the Γ 's correspond to the spin direction of Fig. 4 or the reversed direction, respectively. The zero corresponds to a magnetically disordered site.

Structure [I (2a), $\Gamma(4f)$]	Structure type	Absent reflections				
		{001}	{002}	{004}	{103}	{112}
(Γ_2^+, Γ_2^+)	FO					
$(-\Gamma_2^+, \Gamma_2^+)$	FI				x	x
(Γ_3^+, Γ_3^+)	AF				x	
$(-\Gamma_3^+, \Gamma_3^+)$	AF					
(Γ_5^+, Γ_5^+)	FO					
$(-\Gamma_5^+, \Gamma_5^+)$	FI		x	x	x	x
(Γ_6^+, Γ_6^+)	AF	x			x	
$(-\Gamma_6^+, \Gamma_6^+)$	AF					
$(0, \Gamma_2^-)$	AF				x	x
$(0, \Gamma_3^-)$	AF					
$(0, \Gamma_5^-)$	AF		x	x	x	x
$(0, \Gamma_6^-)$	AF	x				
$(\pm \Gamma_2^+, \Gamma_3^+)$	FI				x	x
$(\pm \Gamma_2^+, \Gamma_2^-)$	FI					x
$(\pm \Gamma_2^+, \Gamma_3^-)$	FI				x	x
$(\pm \Gamma_3^+, \Gamma_4^+)$	FI				x	x
$(\pm \Gamma_3^+, \Gamma_2^-)$	AF				x	x
$(\pm \Gamma_3^+, \Gamma_3^-)$	AF				x	
$(\pm \Gamma_5^+, \Gamma_6^+)$	FI	x	x	x	x	x
$(\pm \Gamma_5^+, \Gamma_5^-)$	FI	x	x	x		x
$(\pm \Gamma_5^+, \Gamma_6^-)$	FI		x	x	x	x
$(\pm \Gamma_6^+, \Gamma_5^+)$	FI	x	x	x	x	x
$(\pm \Gamma_6^+, \Gamma_5^-)$	AF	x	x	x	x	x
$(\pm \Gamma_6^+, \Gamma_6^-)$	AF	x				x

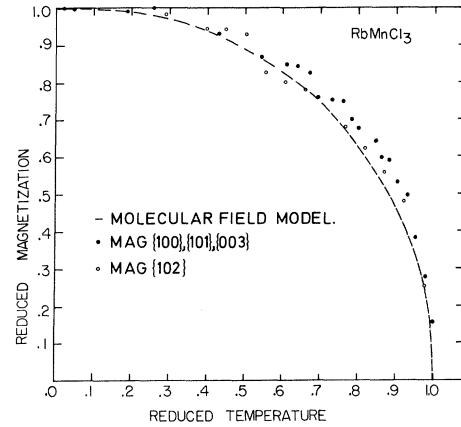


FIG. 6. Reduced-temperature dependence of the sublattice magnetization in RbMnCl_3 derived from the magnetic lines $\{100\} + \{003\} + \{101\}$ and $\{102\}$, compared with the result of molecular field model for Mn^{2+} ($S = \frac{5}{2}$).

Notice that all (24) structures (lower half) not allowed by SOPT are also ruled out by line extinctions. In the fourth and final step we compare the calculated intensities for the three remaining structures with the observed integrated intensities (Table II). The best agreement is obtained with the first of these three structures. The agreement is not as good as one would expect in this type of work. It is suspected that this is due in part to the crystallographic distortion already mentioned. The other two structures are also inconsistent with the finding of Shane *et al.*⁵ which reported that the spin in this compound is perpendicular to the c axis. The increase in the magnetic lines intensities which resulted from the application of an external magnetic field perpendicular to the reflecting planes also implies that the spins are directed perpendicular to the c axis. This leads to the conclusion that the magnetic structure of RbMnCl_3 is $(-\Gamma_6^+, \Gamma_6^+)$. In this structure the spins lie perpendicular to the c axis in ferromagnetic planes; these planes are stacked antiferromagnetically along the c axis in the succession $A(+)$, $B(-)$, $B(+)$, $A(-)$, $C(+)$, $C(-)$.

The magnetic structure factor of the $2a$ sublattice vanishes for the reflection $\{102\}$ so that the only contribution to this line in the neutron-diffraction pattern comes from the $4f$ sublattice. Thus, by measuring the temperature dependence of the $\{102\}$ line, the Néel temperature of the $4f$ sublattice was found to be $(94 \pm 2)^\circ\text{K}$. The other magnetic line $\{100\} + \{003\} + \{101\}$ has contributions from both the $2a$ and $4f$ sublattices; its temperature dependence shows only one transition point (Fig. 3), which is equal to that found from the other line. Hence, the two sublattices have the same Néel temperature showing that they are coupled

TABLE II. Calculated magnetic intensities for three possible magnetic structures compared with the observed integrated intensities. The intensities are normalized with respect to the strongest magnetic line. The observed and calculated intensities (for the three structures) of the lines {001}, {002}, {004}, {103}, and {112} are zero.

{hkl}	Observed	Calculated		
		(-Γ ₆ [*] , Γ ₆ [*])	(-Γ ₃ [*] , Γ ₃ [*])	(0, Γ ₃ ⁻)
100				
003	1000 ± 35	1000	1000	1000
101				
102	332 ± 24	380	534	152
104				
110	207 ± 52	200	113	377
005				
111				
200				
105				
113	915 ± 110	640	990	230
201				
006				
202				
114				
203	64 ± 67	28
106				
204				
007	42 ± 62	51	72	80
115				

magnetically. This is in agreement with the SOPT theory of Landau and Lifshitz. This theory predicts that, when the two sites have the same Néel temperature, they will transform according to the same irreducible representation of the crystallographic space group, which is the case here. The sublattice magnetization as a function of temperature was calculated from the temperature dependence of the intensities of the two mentioned magnetic lines. These results are compared (Fig. 6) with the magnetization M/M_0 calculated in the molecular field model from the equation

$$\frac{M}{M_0} = B_{5/2} \left(\frac{T_N}{T} \frac{M}{M_0} \right),$$

where $B_{5/2}$ is the Brillouin function for $S = \frac{5}{2}$. The

deviation of the experimental data from the molecular field curve is similar to that found for Cr₂O₃¹² and other compounds, and is ascribed to the inadequacy of the molecular field theory. From the relation of the intensity of the {100} + {003} + {101} and {102} magnetic lines at liquid-helium temperature to nuclear intensities, magnetic moments of $3.9 \pm 0.2 \mu_B$ and $4.2 \pm 0.2 \mu_B$, respectively, were deduced.

We have also calculated the anisotropic part of the dipolar energy, E per ion, using

$$6E = -3 \sum_i^{\text{cell}} \sum_j^{\text{cryst}} \frac{(\vec{\mu}_i \cdot \vec{r}_{ij})(\vec{\mu}_j \cdot \vec{r}_{ij})}{r_{ij}^5}$$

for the magnetic lattice ($\mu = 5 \mu_B$, $a = b = 7.164 \text{ \AA}$, $c = 17.79 \text{ \AA}$) of RbMnCl₃. The summation was carried over about 1000 unit cells and resulted $E_1 \sim 0.32 \times 10^{-16}$ erg/ion and $E_{\parallel} \sim 1.91 \times 10^{-16}$ erg/ion for the spins perpendicular and parallel to the hexagonal axis respectively, in qualitative agreement with the proposed structure. The dipolar anisotropy field $H_A = (E_{\parallel} - E_1)/\mu$ is 3430 Oe. The corresponding value calculated by Lee *et al.*⁷ for the isostructural ($\mu = 5 \mu_B$, $a = b = 6.213 \text{ \AA}$, $c = 15.074 \text{ \AA}$) CsMnF₃ is 6795 Oe.

According to the diffraction data, the structure may be any linear combination of L_1 and L_2 , where L_1 and L_2 are the basis vectors (Fig. 4) having the orthorhombic symmetries $Cm'c'm$ and $Cmcm$, respectively, which we are using to span the space of Γ_6^* . It is interesting that $Cm'c'm$ allows ferromagnetism F_z in the z direction whereas, $Cmcm$ does not. The Hamiltonian responsible for weak ferromagnetism F_z in conjunction with L_1 will contain invariants of order six¹³ and will be of the form

$$H = AF_z^2 + BF_z L_1^3 \cos 3\phi + CL_1^6 \cos 6\phi,$$

where ϕ is the angle between the antiferromagnetic axis and the vector perpendicular to the plane of the c glide. For this Hamiltonian to be stationary, F_z must vary as L_1^3 . The fact that F_z is allowed with L_1 and not allowed with L_2 brings about an extremely interesting situation. If one were able to detect F_z , with a single crystal, one could also modulate F_z by rotating the crystal around its c axis in a magnetic field perpendicular to \hat{c} .

¹M. Kestigian, W. J. Croft, and F. D. Leipziger, J. Chem. Eng. Data **12**, 97 (1967).

²H. J. Seifert and F. W. Koknat, Z. Anorg. Allgem. Chem. **341**, 269 (1965).

³G. N. Tiskhchenko, Tr. Inst. Kristallogr. Akad. Nauk SSSR **93** (1955).

⁴R. W. Kedzie, J. R. Shane, M. Kestigian, and W. J. Croft, J. Appl. Phys. **36**, 1195 (1965).

⁵J. R. Shane, R. W. Kedzie, and M. Kestigian, J.

Appl. Phys. **37**, 1134 (1966).

⁶S. J. Pickart, H. A. Alperin, and R. Nathans, J. Phys. **25**, 565 (1964).

⁷K. Lee, A. M. Portis, and G. L. Witt, Phys. Rev. **132**, 144 (1963).

⁸S. J. Pickart and H. A. Alperin, J. Appl. Phys. **39**, 1332 (1968).

⁹Tiskhchenko's original paper was not available to us; but we assumed, on the basis of the information given

by Seifert (Ref. 2), that a_0 and c_0 of his unit cell are one and one-third of the respective values given by Seifert.

¹⁰E. F. Bertaut, *Acta Cryst.* **A24**, 217 (1968).

¹¹G. Shirane, *Acta Cryst.* **12**, 282 (1959).

¹²H. Shaked and S. Shtrikman, *Solid State Commun.* **6**, 425 (1968).

¹³E. A. Turov, *Physical Properties of Magnetically Ordered Crystals* (Academic, New York, 1965), p. 134.

Ferromagnetic Spin Excitations in a One-Band Metallic Loop, the Case of Long-Range Interactions

J. Chen and M. Bailyn

Department of Physics, Northwestern University, Evanston, Illinois 60201*

(Received 17 June 1970)

We extend the previous treatment of one-band spin excitations to include an arbitrary band term and a long-range two-body interaction. The system still consists of N electrons in a periodic loop lattice with N sites. It is found that the number of bound states depends on the range of the effective two-body interaction, and that the distribution in energy scale of these bound states depends on the spatial variation of the two-body interaction strength.

In a previous paper,¹ we considered a system of N electrons in a periodic loop potential which has N lattice sites. A one-band Hamiltonian containing a nearest-neighbor interaction was considered, and the one-spin-flip spectra relative to a saturated ferromagnetic eigenstate were calculated exactly.

It was found that the characteristic terms contributing to the spin-wave spectrum are the band term, the correlation term ($\sim n_i n_i$), and the inter-site exchange term. In the present paper we shall extend the treatment to arbitrary band structure and to include more than nearest-neighbor terms for the two-body interaction. The explicit form of the Hamiltonian is as follows²:

$$H = H_b + H_c + H_{ex}, \quad (1)$$

where

$$H_b = \sum_k \sum_\sigma \mathcal{E}_k C_{k,\sigma}^\dagger C_{k,\sigma}, \quad (2)$$

$$H_c = U_0 \sum_{i=1}^N n_{i,+} n_{i,-} + \sum_{i=1}^N \sum_{l=1}^{N-1} U_l (n_{i,+} + n_{i,-}) \times (n_{i+l,+} + n_{i+l,-}), \quad (3)$$

$$H_{ex} = - \sum_{i=1}^N \sum_{l=1}^{N-1} J_l (C_{i,+}^\dagger + C_{i,-}^\dagger C_{i+l,-}^\dagger - C_{i+l,+} + \text{H. c.}) - \sum_{i=1}^N \sum_{l=1}^{N-1} \frac{J_l}{2} (n_{i,+} - n_{i,-})(n_{i+l,+} - n_{i+l,-}), \quad (4)$$

where $C_{i,\sigma}^\dagger$, $C_{i,\sigma}$, $n_{i,\sigma}$ are, respectively, the creation, annihilation, and number operator of the i th Wannier orbital with spin index σ , and $C_{k,\sigma}^\dagger$, $C_{k,\sigma}$ are the Bloch operators with wave vector k , and where

$$U_l = U_{-l} = U_{N+l}, \quad (5)$$

$$J_l = J_{-l} = J_{N+l}.$$

The Wannier and Bloch operators are related by

$$C_{k,\sigma} = N^{-1/2} \sum_{i=1}^N e^{ikh} C_{i,\sigma},$$

$$k = \frac{2\pi}{N} n, \quad n = 0, 1, 2, \dots, (N-1). \quad (6)$$

The band Hamiltonian can be rewritten in terms of Wannier operators as

$$H_b = \sum_{l,m} \sum_{\sigma} V(l-m) C_{l,\sigma}^\dagger C_{m,\sigma}, \quad (2')$$

where

$$V(l) = N^{-1} \sum_k e^{ikh} \mathcal{E}_k. \quad (7)$$

Let $|\phi_0\rangle$ be the state with all Wannier sites occupied by down-spin electrons and with no up-spin electrons, then $|\phi_0\rangle$ is an eigenstate of the Hamiltonian H with eigenvalue

$$E_0 \equiv \langle \phi_0 | H | \phi_0 \rangle = \sum_k \mathcal{E}_k + N \sum_{l=1}^{N-1} (U_l - \frac{1}{2} J_l). \quad (8)$$

Since the Hamiltonian commutes with the total spin of the system, the simplest stable excitation will be where $N-1$ electrons have down-spin, and one electron has up-spin. Let us consider the one-spin-flip states

$$\Psi_{f,g} \equiv C_{f,+}^\dagger C_{g,-} | \phi_0 \rangle, \quad (9)$$

and solve the Schrödinger's equation in the subspace spanned by $\{\Psi_{f,g}\}$,

$$H\Psi = E\Psi, \quad (10)$$

where

$$\Psi = \sum_{f,g} A_{f,g} \Psi_{f,g}, \quad (11)$$